Investigating laser intensity profile and light scattering effects in the transmission laser welding process of 3D printed parts

Thi-Ha-Xuyen Nguyen, André Chateau Akué Asséko, Anh-Duc Le, Benoît Cosson

Journal of Advanced Joining Processes 9 (2024) 100186

Contents lists available at ScienceDirect

Journal of Advanced Joining Processes

journal homepage: www.sciencedirect.com/journal/journal-of-advanced-joining-processes

Investigating laser intensity profile and light scattering effects in the transmission laser welding process of 3D printed parts

Thi-Ha-Xuyen Nguyen, André Chateau Akué Asséko, Anh-Duc Le, Benoît Cosson *

IMT Nord Europe, Institut Mines Telécom, University of Lille, Centre for Materials and Processes, Lille, F-59653 Villeneuve d'Ascq, France

ARTICLE INFO

Keywords:
Transmission laser welding (TLW)
3D printing
Light scattering
Experimental measurement intensity
Analytical model
Thermoplastic

ABSTRACT

Transmission Laser Welding (TLW) is a promising technique for joining thermoplastic and composite components, especially those produced through additive manufacturing or 3D printing processes. However, achieving optimal welding quality and efficiency in TLW of 3D printed parts is challenging due to the presence of highly heterogeneous and anisotropic materials, which introduce light scattering and absorption issues. Light scattering is caused by the refraction phenomenon. These phenomena significantly impact the laser intensity profile within the materials and at the welding interface, thereby affecting the energy required for successful welding and the mechanical strength of the final assembly. In this paper, we present an in-depth investigation into the laser intensity profile and the effects of laser-matter interaction on the welding of 3D-printed parts. Our approach combines experimental measurements using a heat flux sensor and an analytical inverse model to measure the laser intensity distribution within the materials at the welding interface. The results obtained from the experimental measurements and numerical identification are compared and analyzed, providing insights into the laser intensity profile in TLW of 3D printed parts.

Introduction

The use of transmission laser welding (TLW) presents numerous advantages in the context of welding thermoplastic polymers and composites for industrial purposes compared to alternative conventional techniques (Asséko et al., 2015; Chabert et al., 2020; Chen et al., 2011; Ghorbel et al., 2009; Wang et al., 2014). TLW offers precision, flexibility, limited heat-affected zone, effortless automation and control, and absence of contamination (Aden, 2016; Le et al., 2023). TLW can be very careful for small series part production. It would be an efficient assembly technique for 3D-printed parts. Combining the two processes: 3D printing and TLW is useful for small series production of personality production. TLW does not need a specific tool, ultrasonic welding, or friction welding. In the family of 3D-printed technologies, you can find the 3D Printed thermoplastics using Fused Deposition Modelling (FDM) (Fig. 1) wherein the mechanical performances are restricted by the fiber orientation within the printing layers, and the relatively low strength of inter-layer bonding (Chacón et al., 2017; Ghorbani et al., 2022; Tian et al., 2016). TLW emerges as a prospective joining technique to form extensive functional assemblies (Le et al., 2023). It allows for producing objects in which the continuous reinforcing fibers are arranged to support multi-directional mechanical loads. The production of complex, customized, high-performance 3D-printed structural parts using TLW remains a challenge today.

In TLW, two thermoplastics components are used: one is transparent at the laser wavelength and the other is absorbent at the same wavelength. Before the welding process starts, the components are aligned together. Then, the laser beam energy passes through the transparent material and gets absorbed into the interface of both materials (Fig. 2). This heats up the interface of the substrate and triggers the melting and fusion of the materials, resulting in a bond creation between the two parts when the temperature is greater than the melting point in this area. The well-established bonding strength between welded parts depends on both an optimal temperature distribution within the heat-affected zone and a controlled welding time.

One of the critical factors influencing the success of TLW of two components is the laser intensity profile within the materials and at the welding interface. Accurate estimation of the laser intensity profile is essential to determine the heat source reaching the interface and to predict the temperature field during the welding process. The temperature distribution and weld profile at the interface were widely determined by numerical simulations (Ilie et al., 2009; Labeas et al., 2010; Le

* Corresponding author.
E-mail address: benoit.cosson@imt-nord-europe.fr (B. Cosson).

https://doi.org/10.1016/j.jajp.2024.100186
Received 21 September 2023; Received in revised form 18 December 2023; Accepted 6 January 2024
Available online 7 January 2024

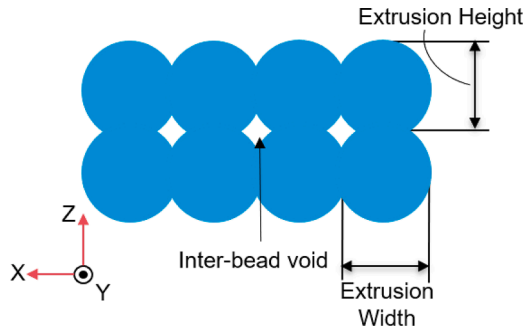

Fig. 1. 3D Printed Polyethylene Terephthalate Glycol (PETG) using Fused Deposition Modelling.

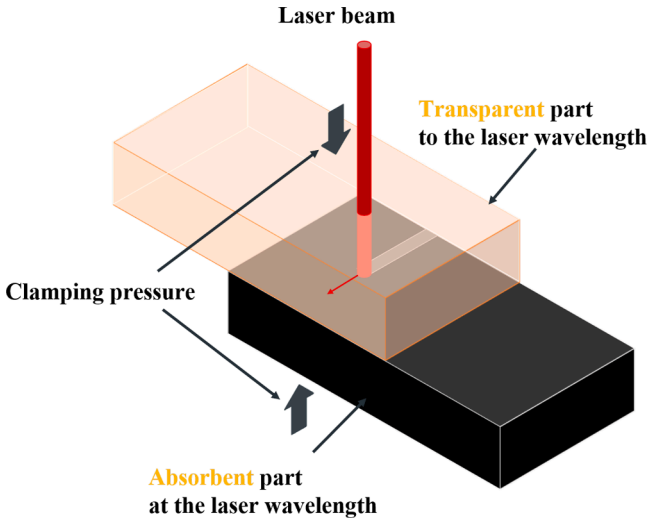

Fig. 2. Transmission Laser welding (TLW).

et al., 2023). Validation was achieved indirectly through infrared thermography measurement at the back surface of the absorbent part (Cosson et al., 2015; Le et al., 2023). Nevertheless, numerical simulations require knowledge of the intensity flux at the weld interface, which depends on the intensity flux distribution of the incident laser beam as well as the thickness, structure, and optical properties of the transparent part. Compared to laser welding of pure polymer, the presence of highly heterogeneous and anisotropic materials introduces a new challenge. Due to these heterogeneities, new phenomena involved in parallel: light scattering and absorption (Fig. 3a). 3D Printed parts have a complex heterogeneous microstructure with porosities and joint zones at material interfaces due to the deposition of successive molten layers.

The scattering phenomenon is responsible for deviations in the laser beam path, resulting in a reduction in energy, uneven distribution, and poor-quality welds. TLW of pure transparent components transmits almost all the energy at the interface (Fig. 3b).

For transparent thermoplastics used in laser welding, the laser intensity profile can be determined through direct measurement of the laser beams intensity flux distribution, also known as beam profiling). Many studies report the TLW measurement transmission, reflection, and light scattering. The main research methods for light scattering include the non-contact scanning method, ray tracing method, analytic model, etc. Jansson et al. (2003) considered the influence of the variable of the welding parameters on the laser weld quality during the laser transmission welding of plastics. Liu et al. (2016). discussed knife-edge and non-contact line scanning experiments to obtain the normalized power flux distribution (NPFD) considering light scattering. Plass et al. (1997) used an inverse method to measure the beam profile from knife-edge data. Zak et al. (2010) proposed a novel experimental technique to measure the light scattering of the laser beam caused by the laser-transparent part in TLW. Zhou et al. (2022) showed the effect of scanning strategies due to the utilization of the three-dimensional finite element modeling for additive manufacturing of Ti-6Al-4V. AkuéAsséko et al. (2015) presented analytical models for laser beam scattering in thermoplastic composites. Besides, the laser intensity at the weld interface was described and optimized for good weldability. These investigations have researched the energy distribution at the weld interface (considering light scattering).

During the thermoplastic TLW process, the laser beam passes through a series of interfaces, among air, quartz, and transparent or semi-transparent parts (as depicted in Fig. 4a) prior to reaching the weld interface. At each interface, the initial laser beam undergoes modification as a result of refraction and reflection phenomena. As a consequence, the initial intensity and surface distribution of the beam are altered. Therefore, utilizing laser beam profiling for direct measurements of the laser power profile at the weld interface (Fig. 4b) is not appropriate as it does not account for these various interfaces.

Temperature was determined using the thermocouple sensors. After that, three-dimensional heat transfer analysis, utilizing the finite element and an inverse method, computed the numerical temperature value at the interface and subsequently estimated the $P_{interface}$ and

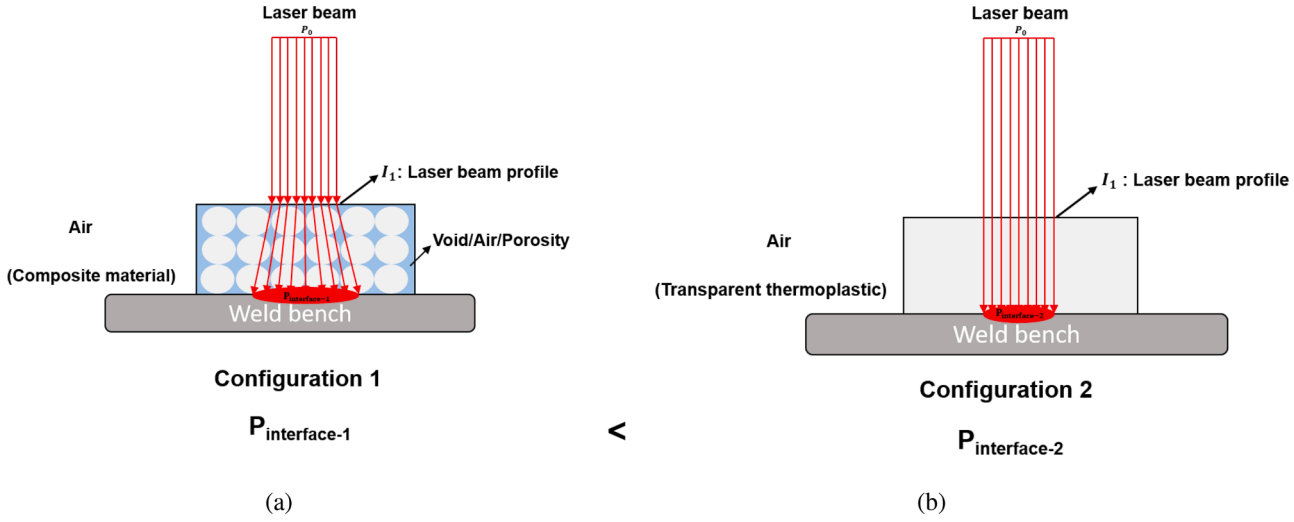

Fig. 3. Identification of the beam laser distribution at the interface: (a) Composite material (b) Transparent thermoplastic.

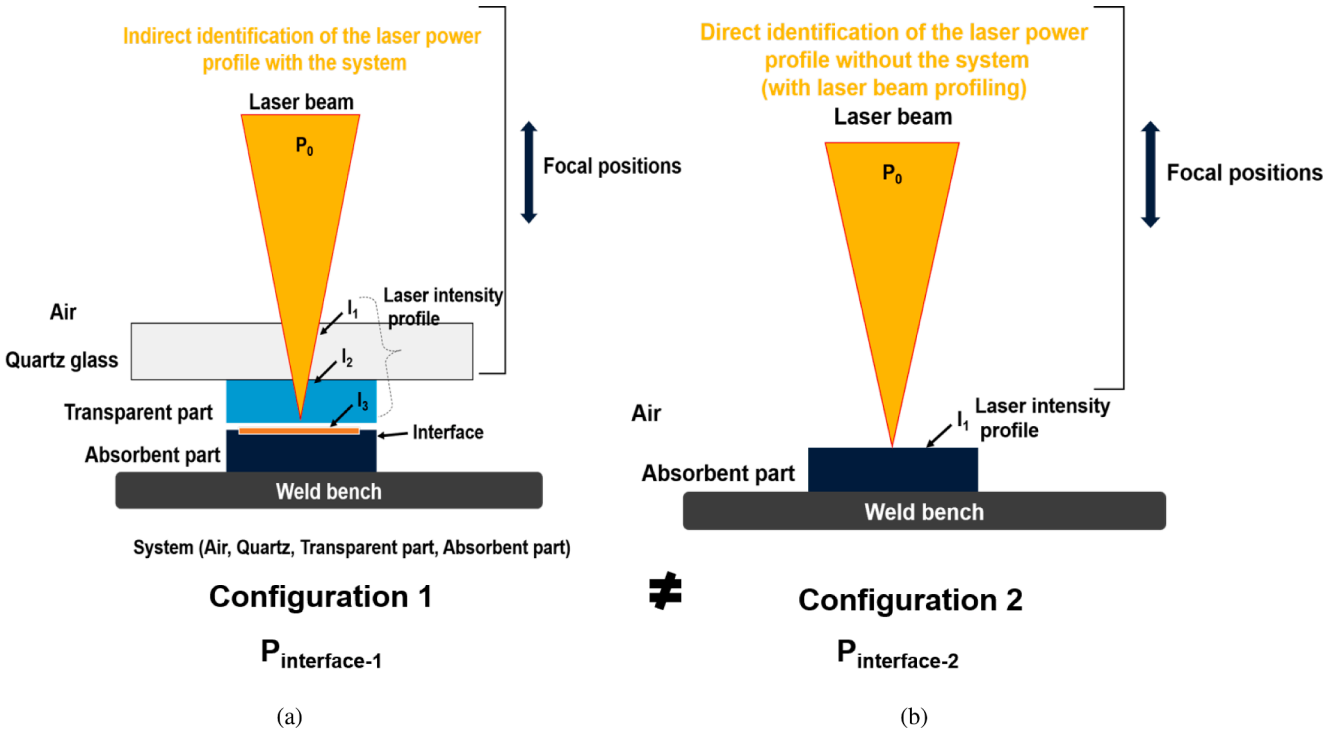

Fig. 4. Identification of the laser intensity distribution at the weld interface: (a) Configuration 1: Indirect method (proposed method) (b) Configuration 2: Direct method with beam profiling.

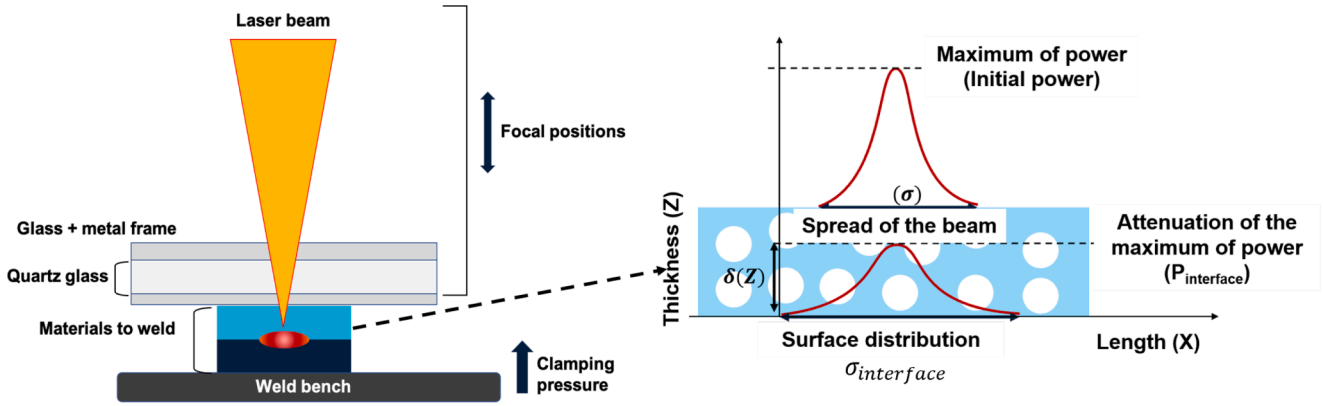

Fig. 5. Laser power measurement at the welding interface.

$\sigma_{interface}$ at the welded zone. This method involves thermal simulation of TLW. The thermal properties of the materials must be known, in the case of heterogeneous materials such as composites, the latter must be homogenized. Most of these methods are time-consuming and have many steps.

This paper aims to propose a new technique that enables the identification of the actual laser power ($P_{interface}$) and real surface distribution ($\sigma_{interface}$) of the laser beam at the weld interface. All the interfaces (Fig. 5), crossed by the laser, affect the surface distribution by light scattering effects. This technique measures the experimental laser power at the welding interface using a heat flux sensor (Fig. 6) before using analytical models of laser welding (AkuéAsséko et al., 2015) to estimate the real power and surface distribution at the welding interface through an inverse method. To validate all those developments, numerical simulations of the temperature field during TLW are carried out. Those simulations would show the effects of light scattering on the size of the heat-affected zone.

TLW modelling

Experimental setup

The 3D-printed specimens used for the welding experiments in this study were made out of Polyethylene Terephthalate Glycol (PETG). The natural transparent PETG was used for the semi-transparent. The materials were supplied by Polymakerin the form of 1.75 mm diameter filaments. According to the supplier, the material has a density of 1.25 g/cm^3 and a glass transition temperature of 81°C. The nozzle temperature is recommended in the range of (230–260°C). The 3D CAD models used to manufacture the welding specimens have a rectangular bar shape of 60 × 40 × 2 mm^3. The nozzle temperature was $T_n = 240$°C, and the bed temperature was $T_b = 75$°C. The printing speed was 30 mm/s and the layer thickness was 0.3 mm. The fill density was 100%, and the filaments fill type was set to line with an angle of 0°.

The experiments of the TLW were performed using the laser welding machine (LEISTER NOVALAS), which was equipped with a diode laser

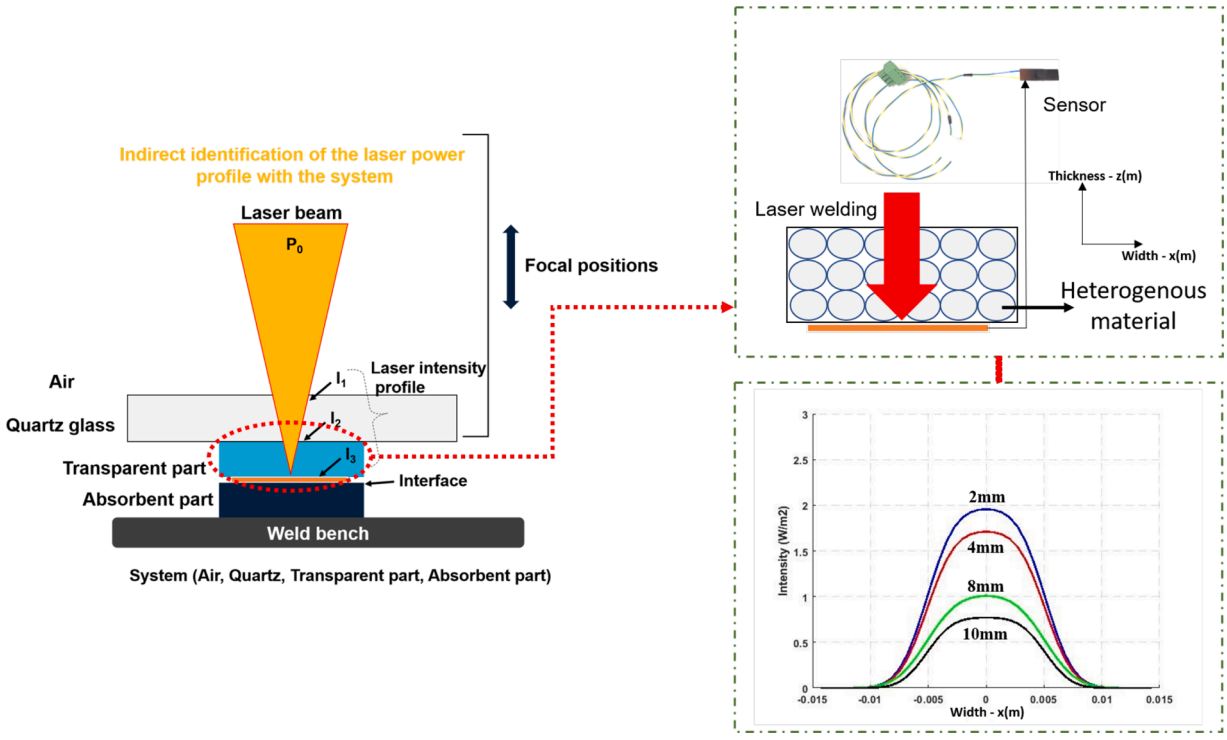

Fig. 6. Identification of the laser intensity distribution at the welded interface.

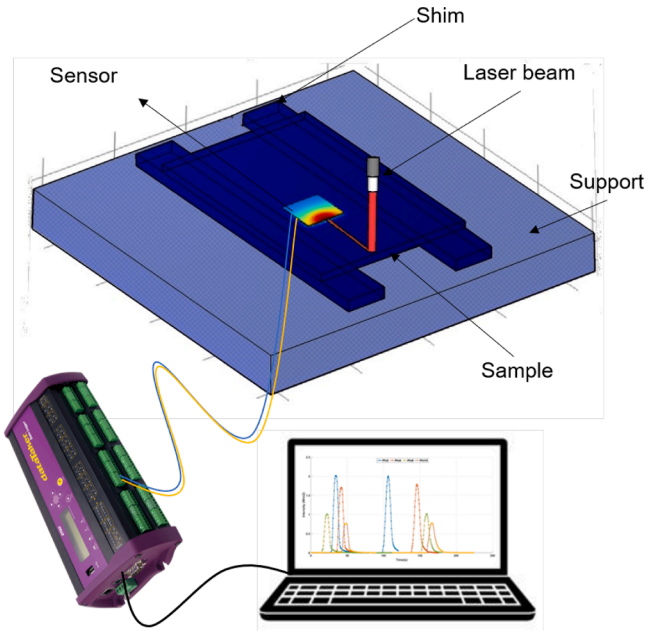

Fig. 7. Schema of experimental set up for flow sensor experiment.

transported by an optic fiber (wavelength of 0.940 μm). The used laser power was set at 10 W in the welding system, the clamping pressure was 6 bar in the pneumatic system. The focal spot had a circular shape and the focal position was varied between 72 mm and 52 mm. This focal spot measured precisely 4 mm. The semi-transparent PETG was irradiated by a laser beam of specific power and two sequences of scan lines were made at a scan speed of 1.36 mm/s. Simultaneously, the laser power profile at the interface of the PETG samples was measured via a heat flux sensor and recorded using the Datataker DT85M data logger device (as illustrated in Fig. 7). The surface and the sensitivity of the sensor were set at 10×10 mm^2 and 1.34 ($\mu V/(W/m^2)$) respectively. The frame rate for capturing the laser power at the interface was 60 Hz, and the measurement uncertainty was ± 0.3 ($\mu V/(W/m^2)$). During TLW of PETG, the laser light is scattered considering the printing paths (line with an angle of 0° and 90°) as an effect of the 3D-printed part micro-structure. The laser beam is only scattered in the traverse or perpendicular direction of the deposited filament (see Fig. 8).

Fig. 8 shows the difference between two weld seams where the welding parameter settings are identical (in the case of a unidirectional part). The only change lies in the direction of the deposited filaments. In the first case, the laser beam displacement is parallel to the filament direction, while in the second case, it is orthogonal to the filament direction.

Virtual model of experiment

Laser scattering models

Different ways are available to model the light scattering using the ray tracing method. A possible way is the numerical simulation of the optical path of the laser through the semi-transparent part. The numerical simulation of ray tracing for laser beam intensity at the welding interface of semi-transparent composites requires considerable computation time due to the scattering within these materials (AkuéAsséko et al., 2015; Cosson et al., 2018; 2015). Describing the heat source at the welding interface is one of the most critical parameters in characterizing the laser welding process. Several analytical approaches exist to depict laser scattering in composite materials. The Beer-Lambert law is suitable for absorbing polymers but not for weakly absorbing and highly scattering media. However, thermoplastic composite materials are inherently scattering due to their heterogeneous nature. Consequently, the Beer-Lambert law is modified to describe the total power distribution of the laser beam in heterogeneous media.

An analytical model has been developed to point out laser power in semi-transparent composites rapidly and at the welding interface (AkuéAsséko et al., 2015; Chen et al., 2011; Le et al., 2023). The parameters of this model can be identified using experimental measurements based on the optical method (Le et al., 2023), making it a valuable

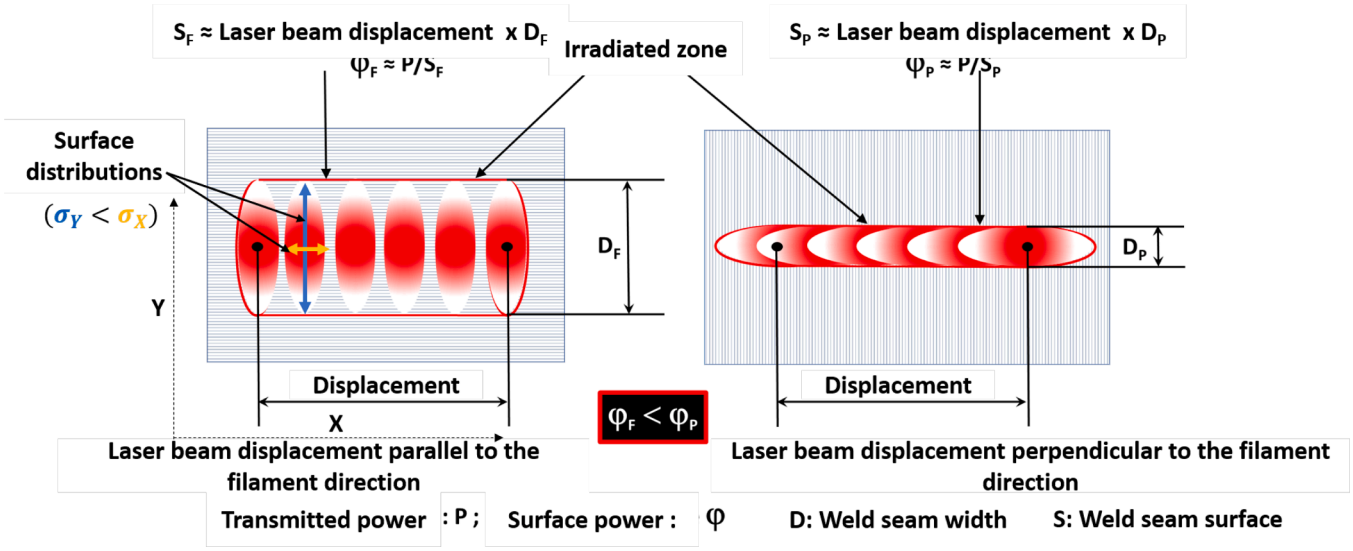

Fig. 8. Influence of laser displacement on energy density in a unidirectional composite depending on filament direction.

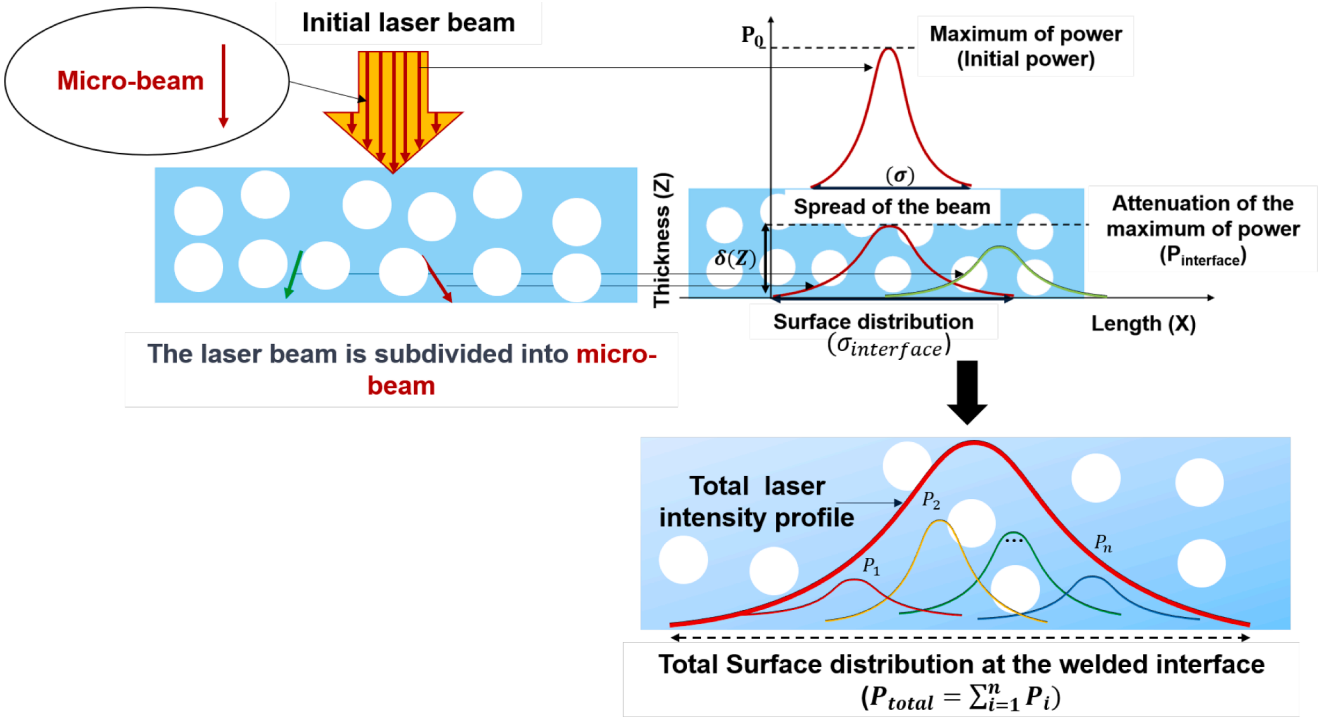

Fig. 9. Attenuation of laser beam intensity at the weld interface due to scattering and absorption during transmission through a heterogeneous medium.

tool for industry professionals. This provides a faster and more efficient alternative to the ray tracing method reserved for advanced research.

The implementation of the model requires several assumptions (see Fig. 9):

- Collimated laser beam
- Gaussian diffusion (light scattering phenomenon) of the beam
- Homogeneous optic properties at the macro-scale
- Diffusion dependent only on the penetration depth (thickness of the part)

The profile of the initial laser beam power $q_r(x,y)$ is described by its total power P (Eq. (1)) and a distribution function (Eq. (2)). The distribution function $f_n(x,y)$ provides the shape of the laser beam's cross-sectional area, such as Gaussian or uniform, for example (Fig. 10). The macroscopic laser beam could be assumed as the sum of the "micro-beam". All these micro-beams have the same behavior and are assumed to be unidirectional. The micro-beam can be decomposed into two parts: the incoming flux, i.e. the one reaching the welding interface, which is presented in this paper, and a founding flux (not presented). This model is applicable to diffusing parts that are non-absorbent.

$$q_r(x,y) = P \times f_n(x,y) \tag{1}$$

$$\int_S f_n(x,y)\,\mathrm{d}x\mathrm{d}y = 1 \tag{2}$$

For a localized micro-ray $(x_0;y_0)$, the Gaussian diffusion is expressed as follows:

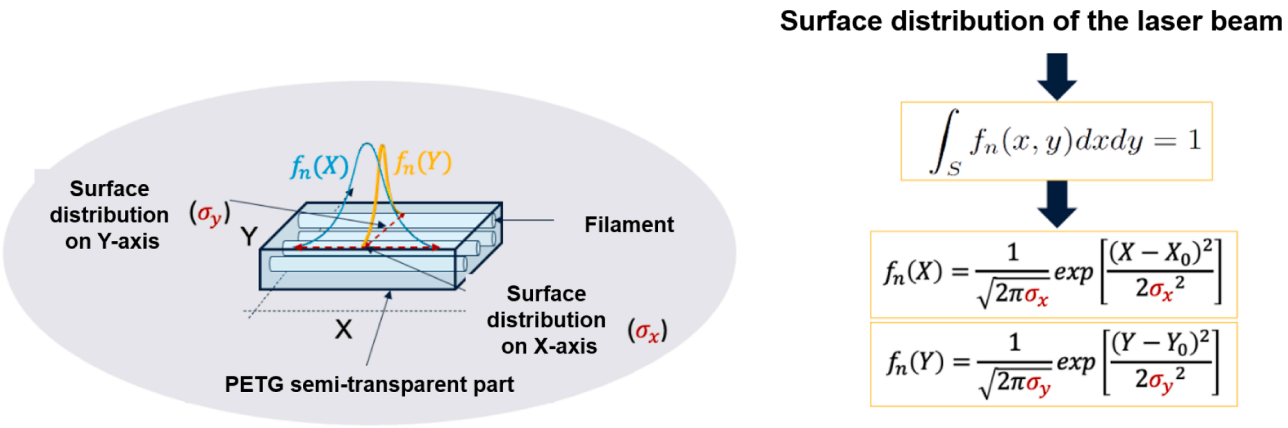

Fig. 10. Light scattering in unidirectional semi-transparent PETG.

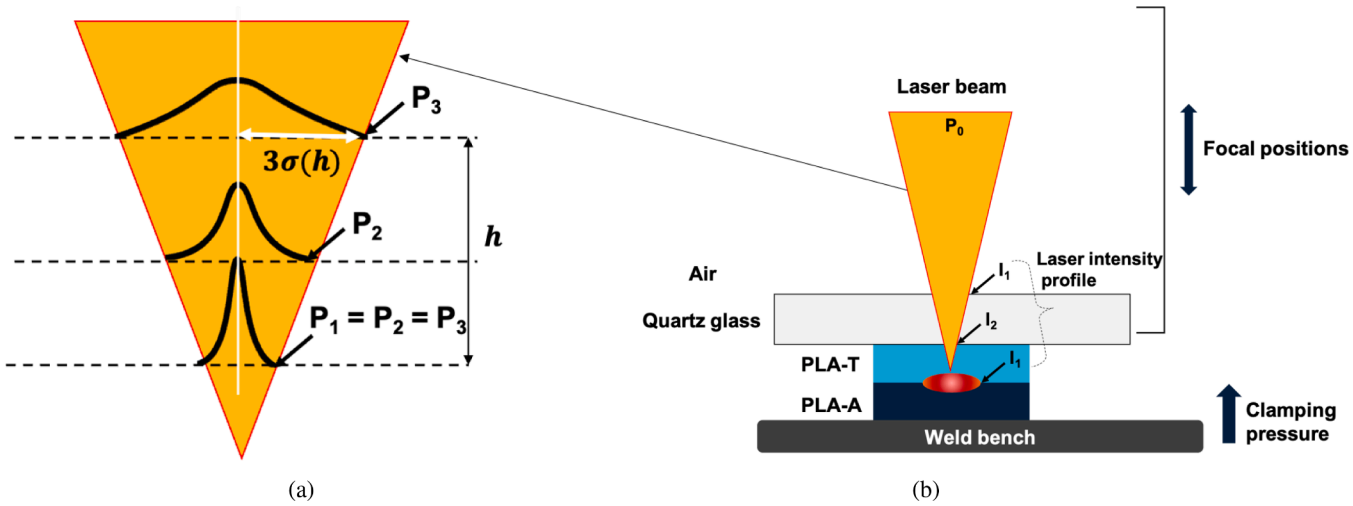

Fig. 11. Identification of the beam laser distribution at the interface: (a) Composite material (b) Transparent thermoplastic.

$$G[(x-x_0),(y-y_0)] = g(x-x_0) \times g(y-y_0) \tag{3}$$

Where:

$$g(x-x_0) = \frac{1}{\sqrt{2\pi}\sigma_x}\exp\left[-\frac{(x-x_0)^2}{2\sigma_x^2}\right]$$
$$g(y-y_0) = \frac{1}{\sqrt{2\pi}\sigma_y}\exp\left[-\frac{(y-y_0)^2}{2\sigma_y^2}\right] \tag{4}$$

G is the 2D Gaussian function that can be expressed as a product of two 1D Gaussian functions with parameters depending on the diffusion direction (x or y). For z=0, at the entrance to the semi-transparent medium, there is no diffusion. Therefore, $\sigma_x = \sigma_y = 0$, and the Gaussian function tends toward the Dirac function, and Eq. (5) is still satisfied. In the general case, for $z \neq 0$, we have $\sigma_x \geq 0$ and $\sigma_y \geq 0$. However, in the case of a unidirectional semi-transparent PETG with filaments oriented solely in the x-direction, we have $\sigma_y = 0\ \forall z$. The surface power profile at the welding interface can be calculated using the following equation as in AkuéAsséko et al. (2015):

$$I(x,y,e) = P \times \delta(e) \times \int_S f_n(x_0,y_0) \times g(x-x_0) \times g(y-y_0)dx_0dy_0 \tag{5}$$

With AkuéAsséko et al. (2015):

$$\delta(e) = \exp(-D \times e) \tag{6}$$

Where e is the thickness of the composite and D is the light scattering coefficient.

In the case of a Gaussian laser beam, the surface distribution function can be expressed in terms of its initial radius $r_0 \approx 3\sigma_0$ (initial spread). $\delta(e)$ is the light scattering ratio. As reported in the literature, some studies (Le et al., 2023; Xu et al., 2015; Zak et al., 2010) have demonstrated that δ decreases exponentially. X, Y, and Z are the cartesian coordinates.

$$f_{ng}(x,y) = \frac{1}{\sqrt{2\pi}\sigma_0}\exp\left[-\frac{x^2+y^2}{2\sigma_0^2}\right] \tag{7}$$

Similarly, to function G (Eq. (3)), function f_{ng} (Eq. (7)) can be decoupled into two independent functions in x and y. Once the decoupling is performed, it is possible to calculate the integral of Eq. (5) and obtain the exact form of the power intensity at the weld interface (Eq. (8)) (AkuéAsséko et al., 2016).

$$I_g(x,y,e) = \frac{P_0 \times \exp(-D \times e)}{2\pi\sigma_0\sqrt{(\sigma_x^2(e)+\sigma_0^2)}} \times \exp\left[-\left(\frac{x^2}{2(\sigma_x^2(e)+\sigma_0^2)} + \frac{y^2}{2\sigma_0^2}\right)\right] \tag{8}$$

It is observed that in the case of an initial Gaussian distribution function, the shape of the heat source at the weld interface remains Gaussian. The same calculations can be performed analytically for a unidirectional

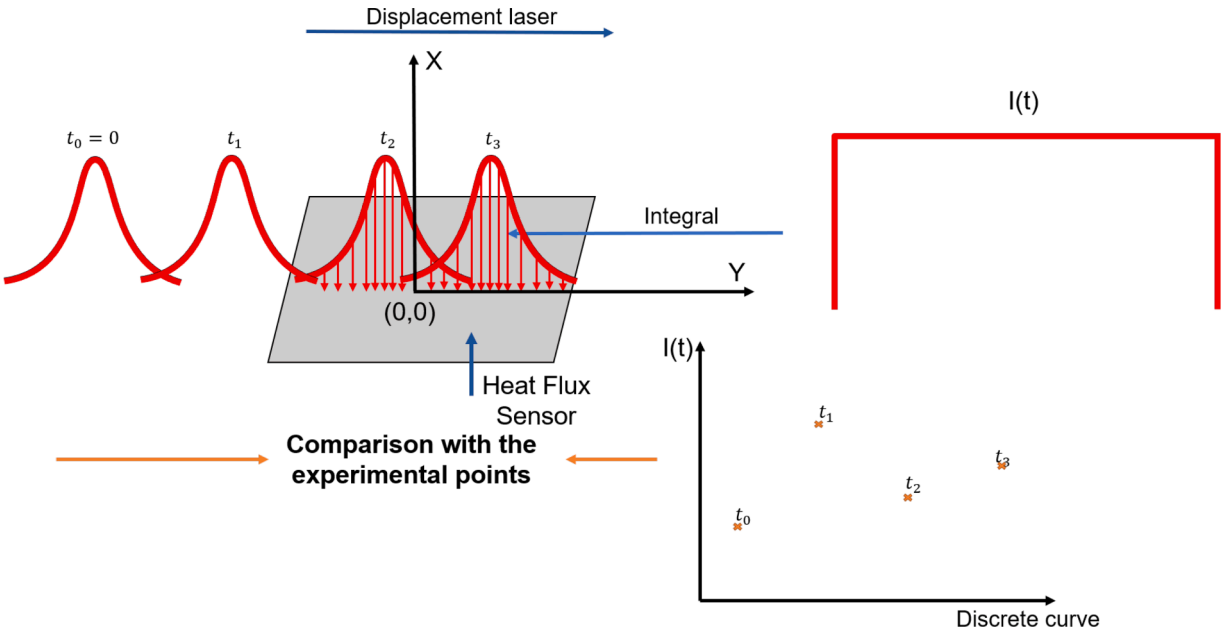

Fig. 12. Radiative flux measurement simulation.

semi-transparent PETG part and an initial uniform circular laser distribution with radius r_0. The result is provided in Eq. (9) using the Gaussian error function (*erf*). For other cases, the integration of Eq. (5) must be performed numerically (AkuéAsséko et al., 2015).

$$I_u(x,y,e) = \frac{P_0 \times \exp(-D \times e)}{2\pi r_0^2} \times \left[-erf\left(\frac{\left(x - \sqrt{r_0{}^2 - y^2}\right)}{\sqrt{2}\sigma_x(e)}\right) + erf\left(\frac{\left(x + \sqrt{r_0{}^2 - y^2}\right)}{\sqrt{2}\sigma_x(e)}\right)\right] \tag{9}$$

where P_0 is the initial laser power and σ_0 is the initial surface distribution. In the classical model represented by Eqs. ((8) and (9)), there is a lack of knowledge regarding the initial surface distribution of the laser beam and its correct power (as illustrated in Fig. 11a). Additionally, after passing through the quartz, the semi-transparent component, and various interfaces, the power and surface distribution of the laser beam at the interface is altered in comparison to the initial power initial surface distribution (as illustrated in Fig. 11b). To address this issue, a new analytical model represented by Eq. (2) was proposed, which takes into account the direct representation of the laser beam at the interface, in terms of both power and surface distribution. The laser beam power profile at the weld interface is given by:

$$I_g(x,y,e) = \frac{P_{interface}}{2\pi\sigma_0\sqrt{\left(\sigma_x^2(e) + \sigma_0^2\right)}} \times \exp\left[-\left(\frac{x^2}{2\left(\sigma_x^2(e) + \sigma_0^2\right)} + \frac{y^2}{2\sigma_0^2}\right)\right] \tag{10}$$

For a Gaussian laser beam:

$$I_u(x,y,e) = \frac{P_{intarface}}{2\pi r_0^2} \times \left[-erf\left(\frac{\left(x - \sqrt{r_0{}^2 - y^2}\right)}{\sqrt{2}\sigma_x(e)}\right) + erf\left(\frac{\left(x + \sqrt{r_0{}^2 - y^2}\right)}{\sqrt{2}\sigma_x(e)}\right)\right] \tag{11}$$

For a uniform circular laser beam:

To determine the actual laser power ($P_{interface} = P_0 \times \exp(-D \times e)$), the actual surface distribution σ_x at the interface and the actual radius of the spot of the beam laser r_0, this study employed the gaussian and uniform circular distribution models. By using the non-linear square fitting method (Le et al., 2023) and calculating the numerical intensities, these values are identified from the experimental measurements by minimizing the error-squares objective function defined in Eq. 12 :

$$\min_X f(X) = \int_{r=0}^{N} \left| I^{num}(r,X) - I^{\exp}(r,X) \right|^2 dr \tag{12}$$

where I^{num} and I^{exp} are the respective numerical and experimental intensity. X represented the model parameters to be identified, $X = [P_{interface}, \sigma_x, \sigma_y]$ for a Gaussian distribution laser profile and $X = [P_{interface}, r_0, \sigma_x]$ for a uniform circular distribution laser profile.

Heat flux sensor model

To model the radiative flux measurement (Fig. 12), the model describing the laser's radiative intensity (Eq. (12)) is exploited. The center of the laser beam is translated to different positions to model the displacement of the laser over the sensor as presented in section 2.1. The sensor is modeled by integrating the signal in a domain centered at point (0,0) and of size 10 mm x 10 mm, which represents the size of the sensor. When the center of the beam is far from the center of the sensor, the signal integral is zero. On the other hand, when the center of the signal is identical to the center of the sensor, the signal integral is maximum. (For results: say that the maximum is equal to the laser beam power if the sensor area is greater than the laser beam cross-section at the sensor). The parameters of the laser beam model are obtained by minimizing the error between the experimental flux measurement results and the model proposed here.

Thermal model of TLW simulation

The temperature field will differ according to the radiative source applied. If we take a direct calculation without taking diffusion into account, the results will be different from a calculation with diffusion taken into account. This is due to the very different surface of the distribution intensity between the two cases.

COMSOL Multiphysics ® software is a solver for multiphysics simulations using finite elements. This software is used to model heat transfer during transmission laser welding. The heat transfer in the interface of the solid COMSOL is used to model heat transfer in solids by

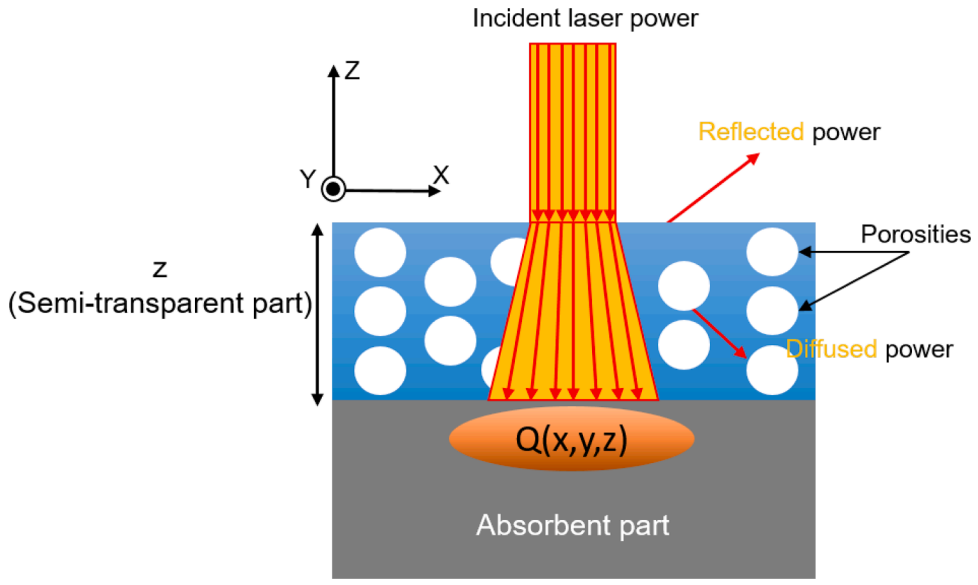

Fig. 13. The heat source of the welded interface during TLW.

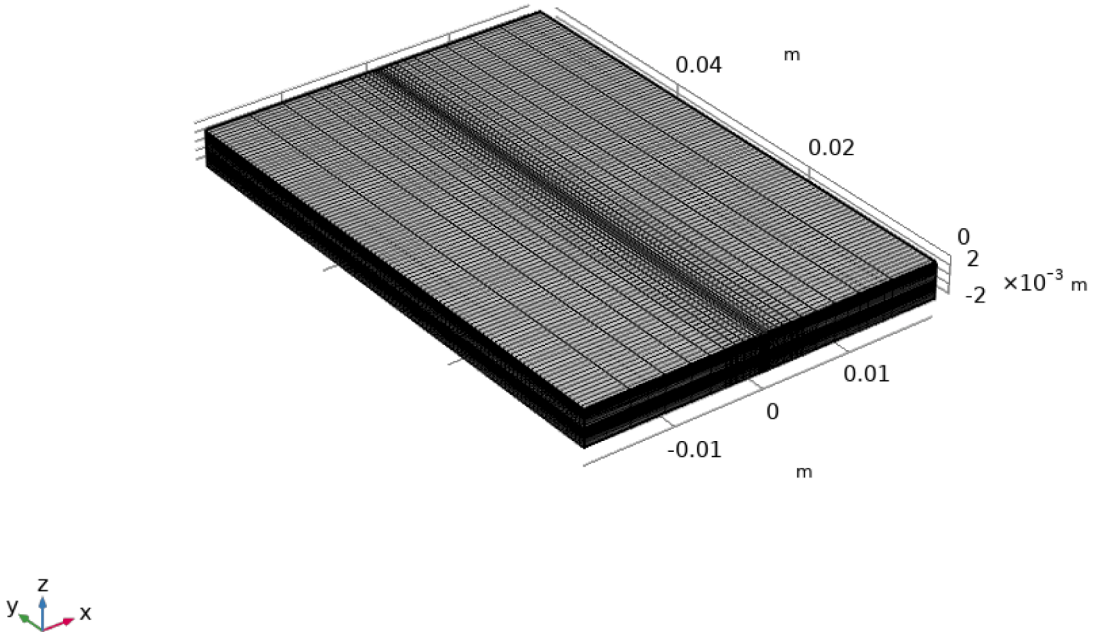

Fig. 14. FEM mesh used in COMSOL for the thermal simulation.

Table 1
Thermal properties of PETG (Hwang et al., 1999; Weber, 2002).

Thermal properties	PETG
Thermal conductivity (k) (W/m.K)	0.2
Density (ρ) (Kg/m^3)	1250
Heat capacity (C_p) (J/Kg.K)	1800

conduction, convection, and radiation. In this study, transmission laser welding is modeled by a radiation source to show the key role of the distribution.

A 3D thermal model of TLW is considered to obtain the temperature field at the interface by solving the energy balance equation (Aden, 2016; Ali et al., 2021; Ilie et al., 2009; Labeas et al., 2010):

$$\rho C_p \frac{\partial T}{\partial t} = -\nabla\cdot(-k\vec{\nabla}T) + Q \tag{13}$$

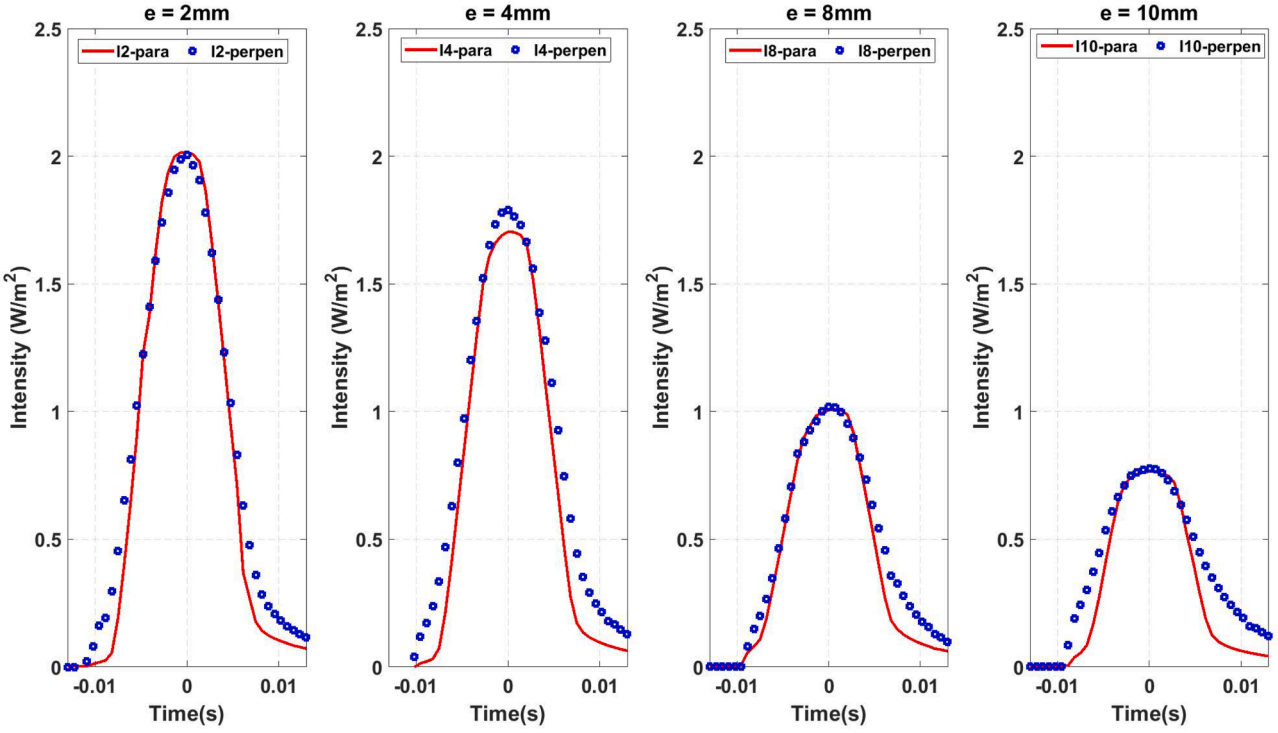

Fig. 15. Output laser beam profiles of the diode laser(Red curve: Filament direction parallel to the laser direction; Blue curve: Filament direction perpendicular to the laser direction.

Table 2
Optimization experiment data of the Gaussian model.

Thickness[mm]	Speed[mm/s]	$D_{sensor}[mm]$	Gaussian beam profile					
-	-	-	$P_{inter}[W]$	$\sigma_x[mm]$	$\sigma_y[mm]$	$P_0[W]$	D $[m^{-1}]$	Error
2	1.36	10x10	**2.13**	**1.91**	**2.87**	**2.63**	**101.45**	**0.67**
4	1.36	10x10	**1.92**	**1.90**	**3.16**	**2.63**	**101.45**	**0.89**
8	1.36	10x10	**1.16**	**2.12**	**3.32**	**2.63**	**101.45**	**0.85**
10	1.36	10x10	**0.99**	**1.75**	**4.17**	**2.63**	**101.45**	**1.71**

Table 3
Optimization experiment data of the uniform circular model.

Thickness[mm]	Speed[mm/s]	$D_{sensor}[mm]$	Uniform circular beam profile					
-	-	-	$P_{inter}[W]$	$r_0[mm]$	$\sigma_x[mm]$	$P_0[W]$	D $[m^{-1}]$	Error
2	1.36	10×10	**2.26**	**3.41**	**2.41**	**2.87**	**107.87**	**0.71**
4	1.36	10×10	**1.95**	**3.35**	**2.70**	**2.87**	**107.87**	**0.46**
8	1.36	10×10	**1.13**	**3.56**	**2.81**	**2.87**	**107.87**	**0.53**
10	1.36	10×10	**1.01**	**3.41**	**3.81**	**2.87**	**107.87**	**0.29**

where ρ is the material density, C_p is the specific heat, T is the temperature, t is the time, k is the thermal conductivity, Q is the heat source and ∇ is the gradient operator.

The laser irradiation is modeled by a volume heat source in the absorbent part with the following equation (AkuéAsséko et al., 2016):

$$Q(x,y,z) = I(x,y,z) \times K_A \times \exp(-K_A \times z) \quad (14)$$

where z is the distance from the interface to the semi-transparent part and K_A is the homogenized absorption coefficient of the 3D printed thermoplastic part. $I(x,y,z)$ is the intensity profile given by Eqs. (10) or (11) (Fig. 13).

A mesh adapted to TLW is constructed to take into account the high-power concentration of the laser beam (see Fig. 14).

The material properties of C_p, ρ, and k are input for semi-transparent material properties. The thermal properties of the absorbent part are that of pure PETG, as seen in Table 1. The initial value for temperature is taken as the default room temperature, 23°C. Thermal insulation is applied on all the faces of the components except the interface. The heat source (Eq. (14)), is determined by the experimental measurements. It is the intensity distribution data that are the radiation source to simulate the temperature field in the COMSOL thanks to the Eq. (13).

The displacement of the laser beam is considered parallel to the printing direction. In this case, that is perpendicular to the welding direction, the diffusion will affect strongly the temperature field.

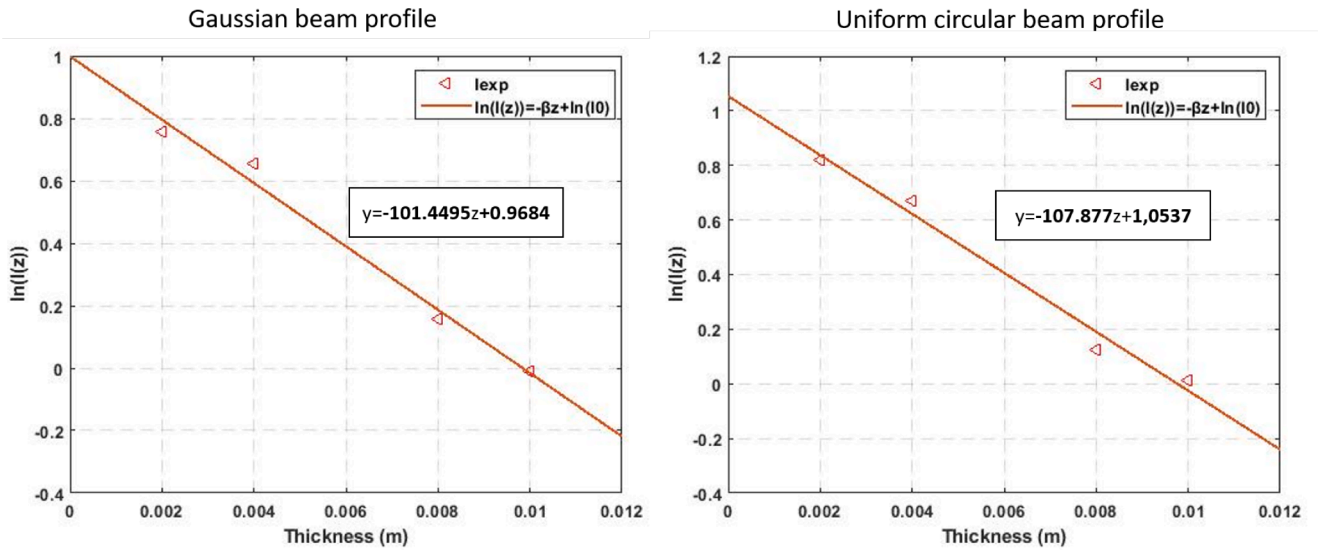

Fig. 16. Normalized intensity log-slope.

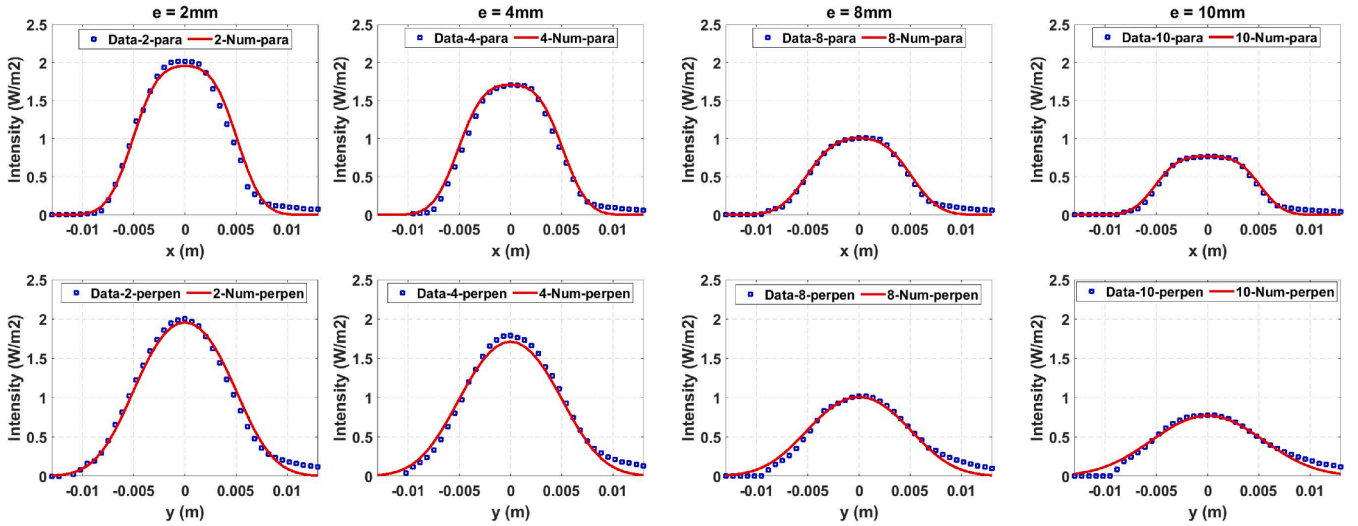

(a) Gaussian model

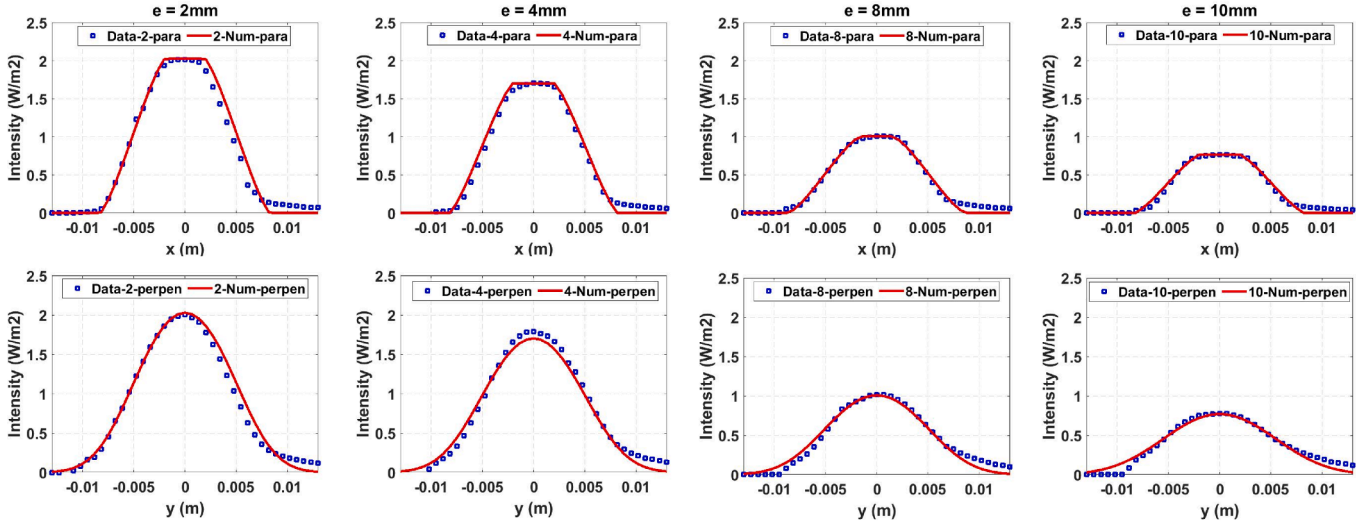

(b) Uniform circular model

Fig. 17. Intensity profiles during the TLW of the 3D-printed part.

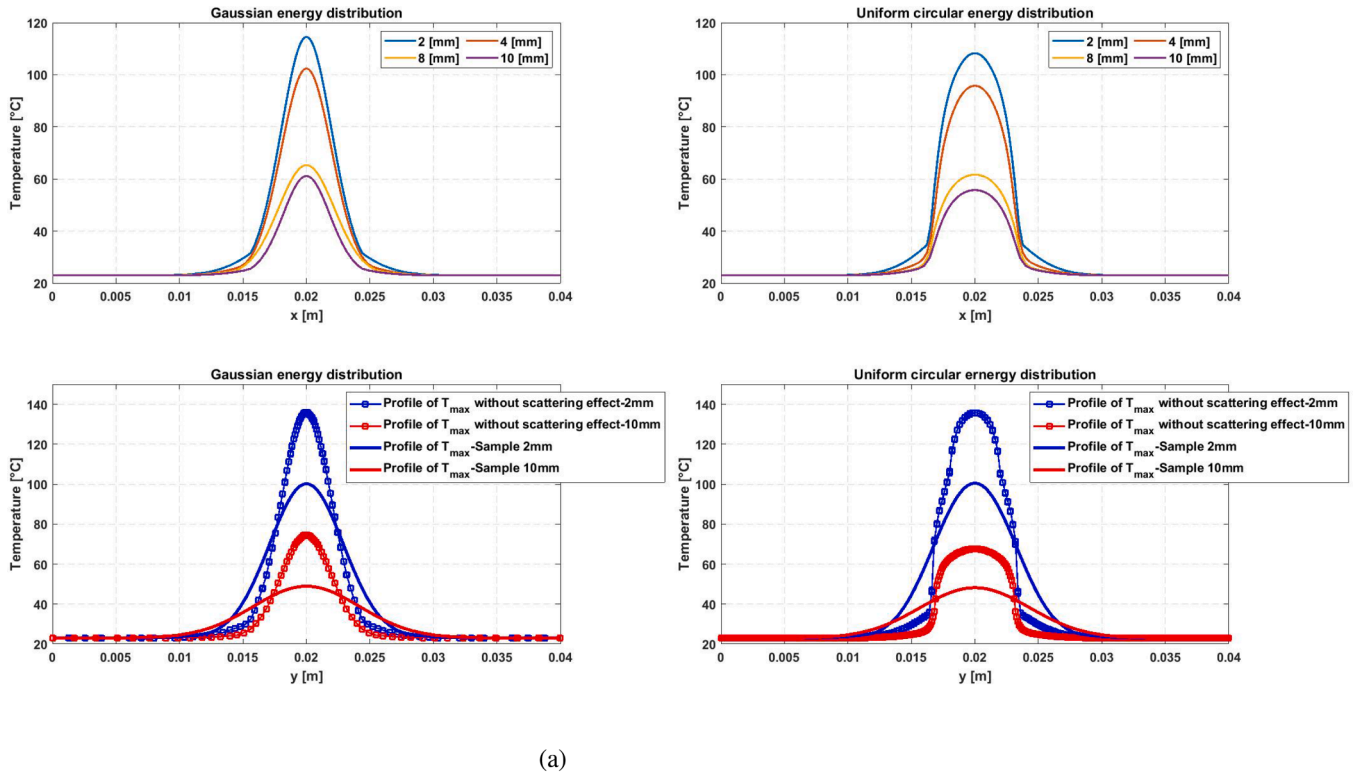

(a)

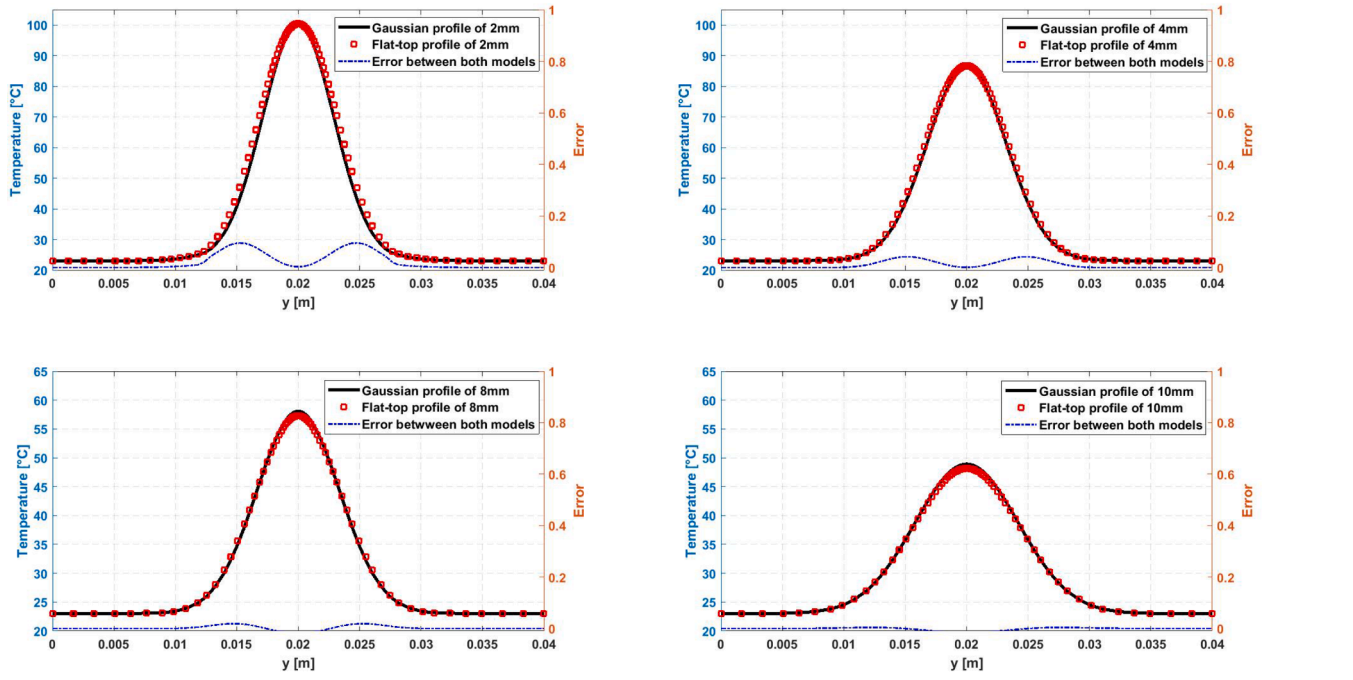

(b)

Fig. 18. Distribution and comparison of the profile of maximum temperature without scattering effect for both samples of 2 mm and 10 mm (b) Comparison of the profile of maximum temperature for two types of energy distribution.

Results and discussion

Experimental results

Fig. 15 illustrated the data in the parallel direction and in the direction perpendicular to the printing direction showing the same maximums but different spreads. The width of the curves depends on the spread of the laser beam, as shown in the article (AkuéAsséko et al., 2015). Here, the laser is only scattered perpendicular to the printing direction. From the peak, values of intensity were measured, as well as

the spread of the beam is related to the light-scattering effect of the 3D-printed part. The power loss is due to both effects: light scattering and absorption. This effect is one of the causes of to reduction in the arrived energy distribution at the interface because the structure of the 3D-printed part is not homogeneous. When the beam laser transmits the sample, a part of the beam laser is refracted because the laser light has to pass the air matrix between two printed layers.

Parameter identifications

The minimization of the error function (Eq. (12)) results is summarized in Tables 2 and 3. The experiments and the modeled profiles obtained by the non-contact scanning method are in good agreement. For both models, the average power of the laser beam is the same for each sample thickness.

Fig. 16 shows the evolution of laser beam attenuation (scattering and absorption) as a function of thickness for both models. The value of the attenuation coefficient (D) is around 100 mm^{-1}. Using the curves in Fig. 16, the initial beam power can be estimated at around 2.7 W.

Fig. 17 shows the experimental results and compares them with the proposed model (Eqs. (10) and (11)) using the parameters derived from error minimization (Eq. (12)) for the different thicknesses studied. Whatever the initial shape of the laser beam used, the model correctly describes scattering in the direction perpendicular to the printing direction. The scattering phenomenon depends on the microstructure of the material and not on the initial shape of the laser beam.

These results demonstrate the importance of scattering in relation to the initial shape of the beam. To demonstrate this importance, numerical simulations of temperature fields are carried out.

Thermal simulations are carried out using the results (Table 1) of the model presented. In Fig. 18, the maximum temperature reached at each point of the weld interface (in a section perpendicular to the movement of the laser beam) is plotted. Some simulations consider the decrease in power as a function of thickness, as well as the associated scattering (flat lines in Fig. 18a-above). Others take into account only the decrease in power without taking into account spreading (dotted line in Fig. 18a-below). Both initial beam shapes, Gaussian and crenelated, are simulated. Fig. 18a shows a significant difference in temperature if diffusion is taken into account or not (between solid and dotted lines). However, the initial shape has very little influence on the result, especially when diffusion is considered.

Fig. 18 b displays the temperature at the weld interface. It shows the comparison between the Gaussian model (blue lines) and the uniform circular model (red lines with dots). The difference between the temperatures obtained for the two models is plotted in blue dotted lines. The difference remains below 10% of the model and decreases as the thickness of the semi-transparent part increases. Indeed, the thickness part, the greater the diffusion. Thus the effect of the initial shape fades with thickness. For the 10 mm thick part, the difference between the two models is of the order of 1%.

Conclusion

The inherent layer-by-layer production of 3D printed thermoplastic technology results in a complex heterogeneous microstructure with a larger amount proposed inside the 3D printed parts. Consequently, laser welding of heterogeneous structures leads to attenuation (scattering and absorption) of the laser beam at the interface. The width of the weld bead is related to the attenuation of the laser beam.

Heavy scattering on thick parts will make it challenging to produce a weld bead. The heat-affected zone's size increases with the semi-transparent part. Diffusion is a function of thickness. As the thickness of semi-transparent parts expands, the energy arriving at the interface decreases, and the spot of the laser beam is enlarged.

We have seen that the laser beam changes its initial shape and its shape at the welding interface. To obtain weld joints of identical quality with the thickness of the part and for a given microstructure, it is necessary to optimize welding parameters such as travel speed, focus point, or initial power.

CRediT authorship contribution statement

Thi-Ha-Xuyen Nguyen: Investigation, Methodology, Software, Visualization, Writing – original draft, Writing – review & editing. **André Chateau Akué Asséko:** Funding acquisition, Project administration, Validation, Visualization, Writing – review & editing. **Anh-Duc Le:** Conceptualization, Formal analysis, Investigation. **Benoît Cosson:** Investigation, Methodology, Software, Supervision, Writing – review & editing.

Declaration of competing interest

The authors declare that they have no known competing financial interests or personal relationships that could have appeared to influence the work reported in this paper.

Data availability

Data will be made available on request.

Acknowledgments

The authors extend their sincere appreciation to the National French Research Agency's ANR JCJC program for funding the SHORYUKEN project (Grant agreement n° ANR-21-CE10-0007-01) through AAPG 2021CE10 æIndustrie et Usine du Futur: Homme, Organisation, Technologiesg initiative. Without their support, this work would not have been possible.

References

Aden, M., 2016. Influence of the laser-beam distribution on the seam dimensions for laser-transmission welding: a simulative approach. Lasers Manuf. Mater. Process. 3 (2), 100–110. https://doi.org/10.1007/s40516-016-0023-x.

AkuéAsséko, A.C., Cosson, B., Deleglise, M., Schmidt, F., Le Maoult, Y., Lafranche, E., et al., 2015. Analytical and numerical modeling of light scattering in composite transmission laser welding process. Int. J. Mater. Forming 8 (1), 127–135. https://doi.org/10.1007/s12289-013-1154-7.

AkuéAsséko, A.C., Cosson, B., Lafranche, É., Schmidt, F., Le Maoult, Y., et al., 2016. Effect of the developed temperature field on the molecular interdiffusion at the interface in infrared welding of polycarbonate composites. Compos. Part B Eng. 97, 53–61. https://doi.org/10.1016/j.compositesb.2016.04.064.

Ali, M.M., Dave, F., Sherlock, R., Mcilhagger, A., Tormey, D., et al., 2021. Simulated effect of carbon black on high speed laser transmission welding of polypropylene with low line energy. Front. Mater. 8.https://www.frontiersin.org/articles/10.3389/fmats.2021.737689

Asséko, A.C.A., Cosson, B., Schmidt, F., Maoult, Y.L., Lafranche, E., et al., 2015. Laser transmission welding of composites-Part A: thermo-physical and optical characterization of materials. Infrared Phys. Technol. 72, 293–299. https://doi.org/10.1016/j.infrared.2015.02.004.

Chabert, F., Garnier, C., Sangleboeuf, J., Akue Asseko, A.C., Cosson, B., et al., 2020. Transmission laser welding of polyamides: effect of process parameter and material properties on the weld strength. Procedia Manuf. 47, 962–968. https://doi.org/10.1016/j.promfg.2020.04.297.

Chacón, J.M., Caminero, M.A., García-Plaza, E., Núñez, P.J., et al., 2017. Additive manufacturing of PLA structures using fused deposition modelling: effect of process parameters on mechanical properties and their optimal selection. Mater. Des. 124, 143–157. https://doi.org/10.1016/j.matdes.2017.03.065.

Chen, M., Zak, G., Bates, P.J., et al., 2011. Effect of carbon black on light transmission in laser welding of thermoplastics. J. Mater. Process. Technol. 211 (1), 43–47. https://doi.org/10.1016/j.jmatprotec.2010.08.017.

Cosson, B., Asséko, A.C.A., Dauphin, M., 2018. Through-transmission laser welding of glass fibre composite: Experimental light scattering identification. AIP Conf. Proc. 1960 (1), 120008. https://doi.org/10.1063/1.5034976.

Cosson, B., Deléglise, M., Knapp, W., et al., 2015. Numerical analysis of thermoplastic composites laser welding using ray tracing method. Compos. Part B Eng. 68, 85–91. https://doi.org/10.1016/j.compositesb.2014.08.028.

Ghorbani, J., Koirala, P., Shen, Y.-L., Tehrani, M., et al., 2022. Eliminating voids and reducing mechanical anisotropy in fused filament fabrication parts by adjusting the

filament extrusion rate. J. Manuf. Processes 80, 651–658. https://doi.org/10.1016/j.jmapro.2022.06.026.
Ghorbel, E., Casalino, G., Abed, S., et al., 2009. Laser diode transmission welding of polypropylene: geometrical and microstructure characterisation of weld. Mater. Des. 30 (7), 2745–2751. https://doi.org/10.1016/j.matdes.2008.10.027.
Hwang, S.-H., Jeong, K.-S., Jung, J.-C., et al., 1999. Thermal and mechanical properties of amorphous copolyester (PETG)/LCP blends. Eur. Polym. J. 35 (8), 1439–1443. https://doi.org/10.1016/S0014-3057(98)00235-3.
Ilie, M., Cicala, E., Grevey, D., Mattei, S., Stoica, V., et al., 2009. Diode laser welding of ABS: experiments and process modeling. Opt. Laser Technol. 41 (5), 608–614. https://doi.org/10.1016/j.optlastec.2008.10.005.
Jansson, A., Kouvo, S., Salminen, A., Kujanpää, V., 2003. The Effect of Parameters on Laser Transmission Welding of Polymers. AIP Publishing. https://doi.org/10.2351/1.5060071.
Labeas, G.N., Moraitis, G.A., Katsiropoulos, C.V., 2010. Optimization of laser transmission welding process for thermoplastic composite parts using thermo-mechanical simulation. J. Compos. Mater. 44 (1), 113–130. https://doi.org/10.1177/0021998309345325.
Le, A.-D., AkuéAsséko, A. C., Nguyen, T.-H.-X., Cosson, B., 2023. Laser intensity and surface distribution identification at weld interface during laser transmission welding of thermoplastic polymers: a combined numerical inverse method and experimental temperature measurement approach. Polym. Eng. Sci.. n/a (n/a). _eprint: https://onlinelibrary.wiley.com/doi/pdf/10.1002/pen.26405.
Le, A.-D., Akué Asséko, A.C., Cosson, B., Krawczak, P., 2023. Investigating the Effect of Interface Temperature on Molecular Interdiffusion during Laser Transmission Welding of 3D-Printed Composite Parts. Materials 16 (18), 6121. https://doi.org/10.3390/ma16186121.
Liu, H., Liu, W., Zhong, X., Liu, B., Guo, D., Wang, X., et al., 2016. Modeling of laser heat source considering light scattering during laser transmission welding. Mater. Des. 99, 83–92. https://doi.org/10.1016/j.matdes.2016.03.052.
Plass, W., Maestle, R., Wittig, K., Voss, A., Giesen, A., et al., 1997. High-resolution knife-edge laser beam profiling. Opt. Commun. 134 (1-6), 21–24. https://doi.org/10.1016/S0030-4018(96)00527-5.
Tian, X., Liu, T., Yang, C., Wang, Q., Li, D., et al., 2016. Interface and performance of 3D printed continuous carbon fiber reinforced PLA composites. Compos. Part A Appl. Sci. Manuf. 88, 198–205. https://doi.org/10.1016/j.compositesa.2016.05.032.
Wang, X., Chen, H., Liu, H., et al., 2014. Investigation of the relationships of process parameters, molten pool geometry and shear strength in laser transmission welding of polyethylene terephthalate and polypropylene. Mater. Des. 55, 343–352. https://doi.org/10.1016/j.matdes.2013.09.052.
Weber, M.J., 2002. Handbook of Optical Materials. CRC Press.Google-Books-ID: 6VpQDoef05wC
Xu, X.F., Parkinson, A., Bates, P.J., Zak, G., et al., 2015. Effect of part thickness, glass fiber and crystallinity on light scattering during laser transmission welding of thermoplastics. Opt. Laser Technol. 75, 123–131. https://doi.org/10.1016/j.optlastec.2015.06.026.
Zak, G., Mayboudi, L., Chen, M., Bates, P.J., Birk, M., et al., 2010. Weld line transverse energy density distribution measurement in laser transmission welding of thermoplastics. J. Mater. Process. Technol. 210 (1), 24–31. https://doi.org/10.1016/j.jmatprotec.2009.08.025.
Zhou, J., Barrett, R.A., Leen, S.B., et al., 2022. Three-dimensional finite element modelling for additive manufacturing of Ti-6Al-4V components: Effect of scanning strategies on temperature history and residual stress. J. Adv. Joining Processes 5, 100106. https://doi.org/10.1016/j.jajp.2022.100106.